

Neural connectivity inference with spike-timing dependent plasticity network

John MOON, Yuting WU, Xiaojian ZHU & Wei D. LU*

Department of Electrical Engineering and Computer Science, University of Michigan, Ann Arbor 48109, USA

Received 2 February 2021/Revised 8 March 2021/Accepted 15 March 2021/Published online 26 April 2021

Abstract Knowing the connectivity patterns in neural circuitry is essential to understand the operating mechanism of the brain, as it allows the analysis of how neural signals are processed and flow through the neural system. With the recent advances in neural recording technologies in terms of channel size and time resolution, a simple and efficient system to perform neural connectivity inference is highly desired, which will enable the process of high dimensional neural activity recording data and reduction of the computational time and cost. In this work, we show that the spike-timing dependent plasticity (STDP) algorithm can be used to reconstruct neural connectivity patterns in a biological neural network, with higher accuracy and efficiency than statistic-based inference methods. The biologically inspired STDP learning rules are natively implemented in a second-order memristor network and are used to estimate the type and the direction of neural connections. When stimulated by the recorded neural spike trains, the memristor device conductance is modulated by the proposed STDP learning rules, which in turn reflects the correlation of the spikes and the possibility of neural connections. By compensating for the different levels of neural activity, highly reliable inference performance can be achieved. The proposed approach offers real-time and local learning, resulting in reduced computational cost/time and strong tolerance to variations of the neural system.

Keywords spike-timing dependent plasticity, neural connectivity, memristor, online learning, second-order memristor

Citation Moon J, Wu Y T, Zhu X J, et al. Neural connectivity inference with spike-timing dependent plasticity network. *Sci China Inf Sci*, 2021, 64(6): 160405, <https://doi.org/10.1007/s11432-021-3217-0>

1 Introduction

Understanding how the brain works is one of the most interesting, but extremely challenging scientific question. Recently, several international brain science programs, such as the BRAIN Initiative in the U.S. [1], the Human Brain Project in the E.U. [2], and the Brain/MINDS program in Japan [3] have been launched to try to map and understand the dynamics of neural activity in the brain. One of the major goals in these programs is inferring neural connectivity patterns from high-dimensional neural activity data recorded by multiple electrode arrays and fluorescence imaging. Knowing the connections between the neurons in the neural system is essential and fundamental information to understand how the signals are processed in the neural system and eventually learn the operating principle of the brain [4, 5].

The human brain has been analyzed at various spatial scales from microscopic level, studying operational mechanisms of single neuron, to macroscopic level, interpreting the connection between the clusters of neurons [6]. In contrast to the simplified pictures in two extreme levels, the mesoscopic analysis, inferring the connections of neurons within the local area, has a large complexity because the human brain consists of more than 86 billion neurons and 1 quadrillion synapses. In addition to the analysis difficulty due to the huge number of possible neuronal pairs, the various types of neurons such as excitatory and inhibitory neurons and the variation of neural parameters such as transmission delay also grow the complexity of mesoscopic analysis. Owing to the difficulty to obtain the true connectivity from the biological neural system, the synthetic data obtained from the spiking neural network with simulated connectivity and other biological properties are widely used to evaluate the inference methods.

* Corresponding author (email: wluce@umich.edu)

Neural connectivity can be inferred by statistical methods [6, 7] including cross-correlation [8], mutual information [9], and transfer entropy [10, 11]. For instance, the cross-correlation measures the strength of the delayed linear relationship between two neurons. The existence and the directionality of excitatory connection can be inferred by detecting a peak profile of cross-correlogram and its time delay, respectively. Since the neural spikes are triggered by the collection of signals of excitatory connections, the excitatory connections can be easily identified by detecting the largest value of cross-correlation or transfer entropy. Compared to identifying the excitatory connections, it is more challenging to infer the inhibitory connections as the statistical methods applied to the neural spike trains, which is a kind of binary datasets, always give us positive outcomes, which make it difficult to distinguish the results of neurons connected by inhibitory synapse from the results of independent neurons. By postprocessing the cross-correlogram [12] or applying the generalized linear model to the cross-correlogram [13], a trough profile of cross-correlogram, which is one of typical fingerprints of inhibitory connections, can be properly detected, and finally both excitatory and inhibitory connections can be inferred.

Although the inference methods based on the statistical measures have been widely used to infer neural connectivity, they have several limitations for analyzing biological neural systems with a large number of neurons and large variations. First, the computational cost for the statistical measures will grow dramatically as the length of neural spike trains and the neural system size increase. For example, the number of possible synaptic connections grows quadratically as the size of the neural system increases. Second, when post processing techniques such as the generalized linear model are applied to the cross-correlogram for inferring both excitatory and inhibitory connections, it is necessary to have a significantly large number of spikes to reliably capture the peak and the trough in the cross-correlogram. Although the required minimum number of spikes depends on the strength of connections and the firing rate of neurons, typically it should be larger than a few thousand spikes for each neuronal spike train [13], which makes it difficult to reduce the computational cost. Third, detecting the specific profile, such as a peak or a trough, in the cross-correlogram is sensitive to the variations of the neural system. Since the model needs to assume several parameters such as a transmission delay to describe the neural system accurately, variations in the system and any mismatch between the assumed parameter and the true parameter will cause the inference accuracy to degrade significantly.

In this paper, we propose a network based on second-order memristors for neural connectivity inference. The second-order memristor [14–16] can natively implement biological features such as spike-timing-dependent plasticity (STDP) [17, 18], which modulates synaptic strength according to the relative timing between the pre- and post-synaptic spikes. Our simulation results using synthetic neural activity data show the STDP algorithm can reconstruct the neural connectivity pattern in the neural network more accurately and more efficiently than statistic-based inference methods. Real-time and local training by the STDP algorithm in turn allow the proposed system to reduce the computational cost/time and offer a strong tolerance to the variation of the neural system.

2 STDP-based inference method

STDP is a synaptic modification process observed in the neural system in animals' brains [17]. According to STDP, the strength of connections between the neurons (i.e., synaptic weight) is adjusted by the relative timing between the spikes of pre- and post-synaptic neurons. A presynaptic spike arriving a few milliseconds before the post-synaptic spike induces the synaptic weight to be strengthened (potentiation), while a presynaptic spike arriving after the post-synaptic spike induces the synaptic weight to be weakened (depression). The origin of STDP can be attributed to the sensitivity of post-synaptic receptors, which is affected by the calcium level, which itself can be elevated by the presynaptic spike. It is believed that STDP plays a key role in the functions of the neural system in the brain, such as signal processing and learning.

Spiking neural networks (SNNs) trained by STDP have already attracted much attention for tasks such as image recognition [19, 20]. Since spike-based approaches are event-based rather than frame-based, the sparsity of input signals allows the SNNs to achieve high power-efficiency with high throughput when compared with conventional deep neural networks. Moreover, local learning rules such as STDP can further reduce the computation cost of training because they do not require error backpropagation which is common in conventional gradient descent learning rules.

In a biological neural system, it is believed that the neural connectivity is developed and refined

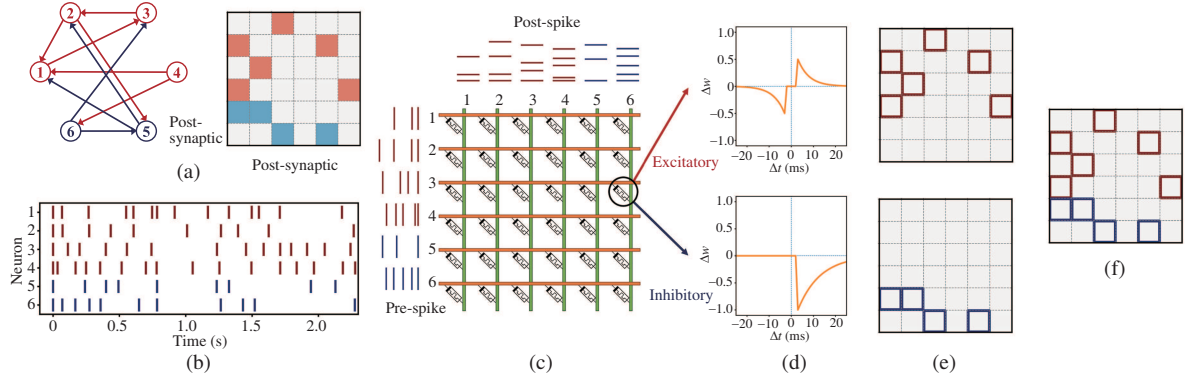


Figure 1 (Color online) Schematic of STDP-based inference methods. (a) Network graph and connectivity matrix. The type and direction of connections are depicted in the network graph as the color (excitatory: red, inhibitory: blue) and direction of the arrow. In the connectivity matrix, the color of the pixel (excitatory: red, inhibitory: blue) shows the ground truth connection from the i th neuron (y -axis) to the j th neuron (x -axis). (b) Raster plot of the spiking neural network simulated by NEST simulator. (c) Overview of STDP-based inference methods implemented in the memristor array. The second-order memristor conductance follows the STDP-based inference method given the series of simulated spike trains. (d) STDP learning rules for excitatory (upper panel) and inhibitory connections (bottom panel). (e) Estimated connectivity matrices for excitatory (upper panel) and inhibitory connections (bottom panel). (f) Final estimated connectivity matrix. Red (blue) squares correspond to the excitatory (inhibitory) connections inferred by the STDP-based inference methods.

by STDP, which adjusts the strength of connections between the neurons based on the relative timing between the spikes of pre- and post-synaptic neurons. During the network evolution, STDP strengthens the connection between the neurons with causality to determine neural circuit functionality and improve signal communication efficiency. Based on the idea that STDP may be able to identify the potential causal relationship between the neurons, in this work, we aim to construct the neural connectivity map from the neural spike trains by using the STDP learning rule.

To evaluate how accurately the STDP-based inference method can reconstruct the connectivity pattern, we simulate the SNNs using the NEST simulator [21] and infer the neural connectivity matrix by applying the simulated neural spike trains on a memristor network consisting of 2nd-order memristors. The inference accuracy is then compared with the statistic-based inference methods, as shown in Figure 1.

Two different versions of SNNs are tested to verify the ability of the STDP-based inference method. One is a simple ternary-weighted network of leaky integrated-and-fire (LIF) neurons with constant ternary synaptic weights: positive for excitatory connection, negative for inhibitory connection, and zero for no connection. Another is a bio-realistic analog-weighted network of Hodgkin-Huxley (HH) neurons, which has log-normal distributed excitatory synaptic weights [22] and normally distributed inhibitory synaptic weights [23]. Once the neural spike trains are obtained from the NEST simulator, they are applied to the second-order memristor array, where the device conduction evolutions are computed either by assuming an ideal device model following the ideal STDP learning rule or by using a physical device model governed by the coupled differential equations. As shown in Figure 1(c), two different STDP learning rules were used for memristor conductance modulation: one for excitatory connection (eSTDP) and another for inhibitory connection (iSTDP). Following the original idea of STDP, the eSTDP potentiates (depresses) the device conductance when a post-spike comes after (before) a pre-spike so that the memristor device corresponding to an excitatory connection between a neuron pair will evolve to a higher conductance compared to others. On the other hand, an inhibitory connection suppresses the activation of the post-synaptic neuron right after the pre-spike. This leads to the absence of post-neuron spikes, and makes it difficult to detect the inhibitory connection via conventional STDP due to the absence of pre-spike and post-spike pairs. Inferring excitatory connections is relatively simple because the contribution of pre-neurons to post-neurons' activation can be estimated from the temporal information of neural activity recording such as the time gap and sequence of pre- and post-spikes. Such temporal information can be processed by both the statistic-based methods such as cross-correlation and the STDP learning rule. This process is, however, only valid when there is a pair of pre- and post-spikes induced by the excitatory connection. When there is an inhibitory connection between neurons, the activation of pre-neuron will suppress the membrane potential of post-neuron and prevent post-neuron from generating the spikes. Thus, to infer inhibitory connections, the inference method should recognize a specific spike pattern that is the activation of pre-neurons followed by the silence of post-neurons. To address this issue, we adopt a

strategy based on the process of elimination. Specifically, the iSTDP rule was developed to depress the device conductance for cases corresponding to excitatory connection or no connection so that the device corresponding to the inhibitory connection will have a higher conductance than other devices in the end. The learning equations of eSTDP and iSTDP are following:

$$\Delta w_{e\text{STDP}} = \begin{cases} \eta_{e\text{STDP}} \times (1 - w_{e\text{STDP}}) \times A_{p,e\text{STDP}} \times \exp\left(\frac{\Delta t}{\tau_{p,e\text{STDP}}}\right), & \Delta t \geq \tau, \\ -\eta_{e\text{STDP}} \times w_{e\text{STDP}} \times A_{d,e\text{STDP}} \times \exp\left(\left|\frac{\Delta t}{\tau_{d,e\text{STDP}}}\right|\right), & \Delta t \leq -\tau, \\ 0, & -\tau < t < \tau, \end{cases} \quad (1)$$

$$\Delta w_{i\text{STDP}} = \begin{cases} -\eta_{i\text{STDP}} \times w_{i\text{STDP}} \times A_{d,i\text{STDP}} \times \exp\left(\frac{\Delta t}{\tau_{d,i\text{STDP}}}\right), & \Delta t \geq \tau, \\ 0, & t < \tau, \end{cases} \quad (2)$$

where $w_{e\text{STDP}}, w_{i\text{STDP}} \in [0, 1]$ are respectively the normalized device conductance for inferring the excitatory and inhibitory connections, $\eta_{e\text{STDP}}, A_{p(d),e\text{STDP}}, \tau_{p(d),e\text{STDP}}$ are respectively the training rate, the amplitude of potentiation (depression), and the time constant of potentiation (depression) of eSTDP, $\eta_{i\text{STDP}}, A_{d,i\text{STDP}}, \tau_{d,i\text{STDP}}$ are respectively the training rate, the amplitude of depression, and the time constant of depression of iSTDP, τ is the transmission delay of the neural network, Δt is the time interval between the pre-spike and the post-spike, $t_{\text{post}} - t_{\text{pre}}$. The amplitude and time constant of STDP rules do not have significant influences on the inference performance, but a small time constant is marginally preferred since the long tails of STDP curves with large time constants can produce more false positives from indirect connections. Here we set the parameters: $\eta_{e\text{STDP}} = 0.2$, $A_{p(d),e\text{STDP}} = 0.5\%$, $\tau_{p(d),e\text{STDP}} = 5$ ms, $\eta_{i\text{STDP}} = 1$, $A_{d,i\text{STDP}} = 1\%$, $\tau_{d,i\text{STDP}} = 10$ ms. Since the iSTDP rule have only depression in contrast to the eSTDP having both potentiation and depression, $w_{e\text{STDP}}$ and $w_{i\text{STDP}}$ are initialized as 0 and 1, respectively.

We note that the final device conductance is affected by the number of pre-spike and post-spike pairs. For instance, the neurons activated more frequently may have a high chance of having a more frequent device conductance updates than the neurons activated less frequently. Thus, to correctly detect the connectivity map across the network using a uniform threshold value, the training rate should be modified according to each neuron's firing rate to compensate for the effects of different neural activity. In general the higher firing rate, the lower the training rate should be. We thus modify the training rate of synapse connecting the i th neuron and the j th neuron as follows:

$$\eta_{ij} = \eta_0 \times \frac{\lambda_{\text{avg}}^2}{\lambda_i \lambda_j}, \quad (3)$$

where η_0 is the initial training rate, and $\lambda_i, \lambda_{\text{avg}}$ are the firing rate of the i th neuron and the averaged firing rate, respectively. We term the STDP-based inference method with (without) the modified training rate 'STDP+' ('STDP0'). After the device arrays trained by the STDP-based inference methods, the optimal threshold for deciding whether there is a specific type of connection or not is determined by maximize the Matthews correlation coefficient (MCC) [24].

$$\text{MCC} = \frac{N_{\text{TP}}N_{\text{TN}} - N_{\text{FP}}N_{\text{FN}}}{\sqrt{(N_{\text{TP}} + N_{\text{FP}})(N_{\text{TP}} + N_{\text{FN}})(N_{\text{TN}} + N_{\text{FP}})(N_{\text{TN}} + N_{\text{FN}})}}, \quad (4)$$

where $N_{\text{TP}}, N_{\text{TN}}, N_{\text{FP}}, N_{\text{FN}}$ are the numbers of true positive, true negative, false positive, and false negative, respectively. A coefficient of +1 represents a perfect classification. The overall inference accuracy, a mean of MCC for excitatory (eMCC) and MCC for inhibitory (iMCC), can then be calculated from comparing the ground truth connectivity matrix and the inferred connectivity matrix.

3 Results

To verify that the STDP-based methods can infer neural connectivity from recorded spike trains, including the type and direction of connections, we first test the inference performance of the STDP-based methods

Table 1 Parameters for ternary-weighted neural network

Neuron parameters			Synapse parameters		
τ_m	20 ms	Membrane time constant	w_{ex}	1 mV	Excitatory weight
τ_r	2 ms	Refractory period	w_{in}	-2 mV	Inhibitory weight
C_m	1 pF	Membrane capacity	τ	3 ms	Transmission delay
V_{reset}	0 mV	Reset potential			
V_{th}	20 mV	Firing threshold			

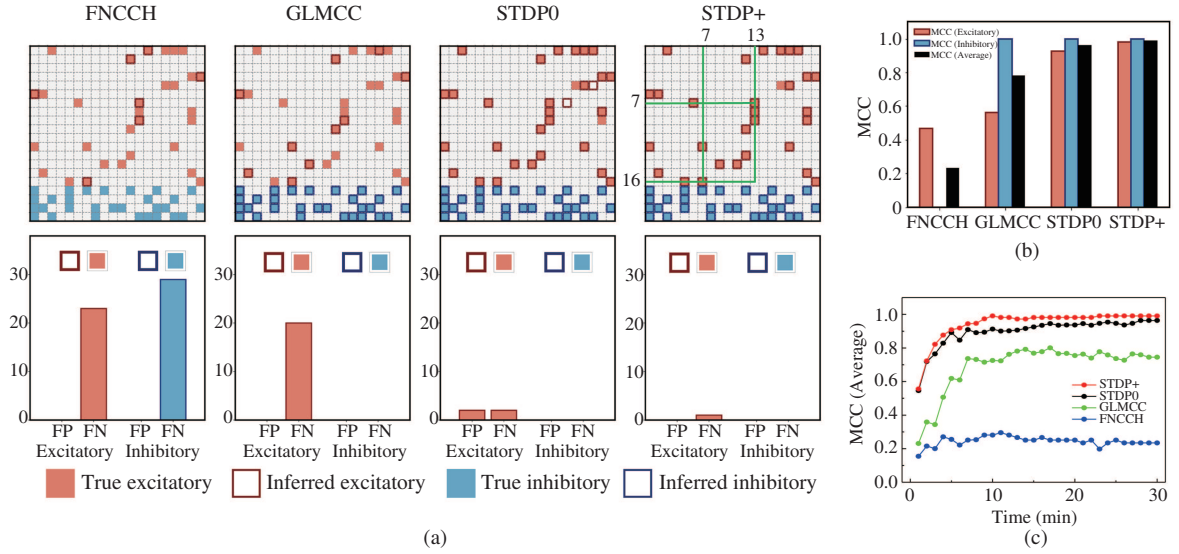


Figure 2 (Color online) Ternary-weighted neural network with LIF neurons. (a) Connectivity matrices (upper panel) with the ground truth (pixel) and the inferred connections (excitatory: red, inhibitory: blue) and the numbers of false positive and false negative cases for the excitatory and inhibitory connections (bottom panel). (b) Inference accuracy in terms of MCC. Averaged MCC is a mean of MCC for excitatory and MCC for inhibitory. (c) Averaged MCCs with respect to the simulation time length.

for a ternary-weighted neural network of LIF neurons. The network consists of 800 excitatory neurons and 200 inhibitory neurons. In the biological neural system, in general only a small portion of the whole neural system can be monitored due to the limited capability of measurement tools. Similarly, we sample 20 neurons (16 excitatory neurons and 4 inhibitory neurons) out of the whole neural population. Each neuron receives the synaptic signals from randomly chosen 100 excitatory neurons and 100 inhibitory neurons. The weights of the excitatory and inhibitory connection, and the transmission delay are assumed to be 1 mV, -2 mV, and 3 ms, respectively. The parameters for the ternary-weighted neural network are summarized in Table 1. The neural network is simulated for a period representing 30 min.

We compare the inference accuracy of the STDP-based methods (STDP0, STDP+) with that of the statistic-based methods such as the filtered normalized cross-correlation histogram (FNCCH) [12] and the generalized linear model with cross-correlation (GLMCC) [13]. Figure 2(a) shows the estimated connectivity matrices and the numbers of false positive and false negative cases for the excitatory and inhibitory connections. The inference accuracies in terms of MCC are summarized in Figure 2(b). FNCCH is based on the normalized cross-correlogram followed by subtracting the mean value of the cross-correlogram. The FNCCH method can distinguish between peaks and troughs by considering the signs: a positive value refers to an excitatory connection, and a negative value refers to an inhibitory connection. The GLMCC method applies the generalized linear model to the normalized cross-correlogram, where the generalized linear model helps distinguish short-range synaptic impacts (i.e., direct connections) from slow, large-scale wavy fluctuations (i.e., noise and indirect connection) by fitting a coupling filter. The STDP-based inference methods outperform the statistic-based methods in inferring both excitatory and inhibitory connections.

Owing to the transmission delay, the STDP-based inference methods can also accurately distinguish the direct connection from the indirect connection. For instance, there are direct excitatory connections from the 16th neuron to the 7th neuron and from the 7th neuron to the 13th neuron. If the inference method is not able to discriminate the direct connection from the indirect connection, it will infer there

is a connection from the 16th neuron to the 13th neuron, which will lead to a false positive in the case of detecting only direct connections. As shown in Figure 2(a), although there is interdependency between the 16th neuron and the 13th neuron due to the indirect connection, the STDP-based inference methods correctly did not mark it as a (direct) connection.

Additionally, the STDP-based inference methods show better tolerance to the randomness of the time interval between the spikes since real-time conductance updates based on STDP, which is a local learning rule and whose effects only become measurable after multiple updates, can largely average out the effect of randomness or fluctuation. On the other hand, FNCCH has a vulnerability to fluctuations in the cross-correlograms since it detects the maximum amplitude of the peak or the trough. If FNCCH detects any peak or trough not caused by the actual connection, it will induce a large number of false estimations as shown in Figure 2(a). Compared to FNCCH, GLMCC has better tolerance to fluctuations by using the generalized linear model to capture the specific profile such as peaks or troughs. Thus, it shows better performance than FNCCH, but still produces worse accuracy than the STDP-based methods in inferring excitatory connections. In particular, GLMCC requires a large number of spikes before it can reliably capture the specific profiles in the cross-correlograms. Figure 2(c) shows the averaged MCCs of the STDP-based methods and the statistic-based methods with respect to the length of simulation time. The more neural spikes, the smoother profile in the cross-correlograms. Thus, the GLMCC inference accuracy improves as a larger number of spikes are applied. On the other hand, the STDP-based methods can produce higher inference accuracy and estimate the correct connectivity matrix using only a smaller number of spikes since it is based on online updates instead of assuming a specific statistical model. Notably, STDP+, which is based on the modulated training rate, shows better performance than STDP0 even for small variations of firing rates, e.g., 4.62 ± 0.28 Hz.

In addition to distinguishing the types of connections, the direction of the connection offers important information to understand how the signal flows in the brain. The transmission delay, which represents the time delay for the neural signal to propagate from one neuron to another, is an important factor in deciding the direction of the connection. While in this work we know the transmission delay in the simulated neural spike data, knowing the exact values of transmission delays for all neurons in the biological neural network is impossible. Since the STDP-based inference methods and the GLMCC methods need to assume the transmission delay value, there will be a high chance of having a mismatch between the true value and estimated value of the transmission delay and the effects of variations in assumed transmission delays thus need to be carefully analyzed.

Figure 3 shows the inferred connectivity matrices with different estimated values of transmission delays. When the estimated value of the transmission delay, 2 ms, is smaller than the true value, 3 ms, the STDP-based methods show slightly degraded inference accuracies but still offer better performance than the statistic-based methods. It is interesting to note that with the underestimated transmission delay the GLMCC method produces almost the same averaged inference accuracy as the GLMCC method with the correct transmission delay. In general, with the underestimated transmission delay, the inference accuracy for excitatory connection is improved, and the inference accuracy for inhibitory connection is degraded. Several individual correlation values can coincidentally be produced within 2 and 3 ms lags in the cross-correlograms. These individual values are caused by noise or random fluctuations rather than by a direct excitatory connection, which results in a wide peak profile. The coincident correlation in the extra margin due to the underestimated transmission delay may help the GLMCC method to capture the peak profile more reliably, but at the same time disturb the GLMCC method to detect the trough profile. When the estimated value of transmission delay, 4 ms, is larger than the true value, 3 ms, the degradation of GLMCC is much significant compared to the degradation of STDP-based methods, as shown in Figure 3(c). With an over-estimated value of transmission delay, the most valuable peaks right after the transmission delay in the cross-correlograms are lost so that GLMCC cannot infer any excitatory connection. The inference accuracy for inhibitory is not degraded much, since the inhibitory connections are stronger than the excitatory connections and produce a wider trough profile wider than the peak profile in the cross-correlograms. Thus, although some parts of the trough profile are excluded due to the overestimated transmission delay, GLMCC can still detect the trough profile in the cross-correlogram. Overall, these results show STDP-based inference methods show stronger tolerance in the mismatch of transmission delay than the statistic-based inference methods.

Typically, biological neural systems have analog synaptic weights rather than ternary synaptic weights. To verify the ability of STDP-based inference methods to reconstruct the connectivity pattern in biological neural systems, we test the system's performance for analog-weighted neural networks with HH neurons.

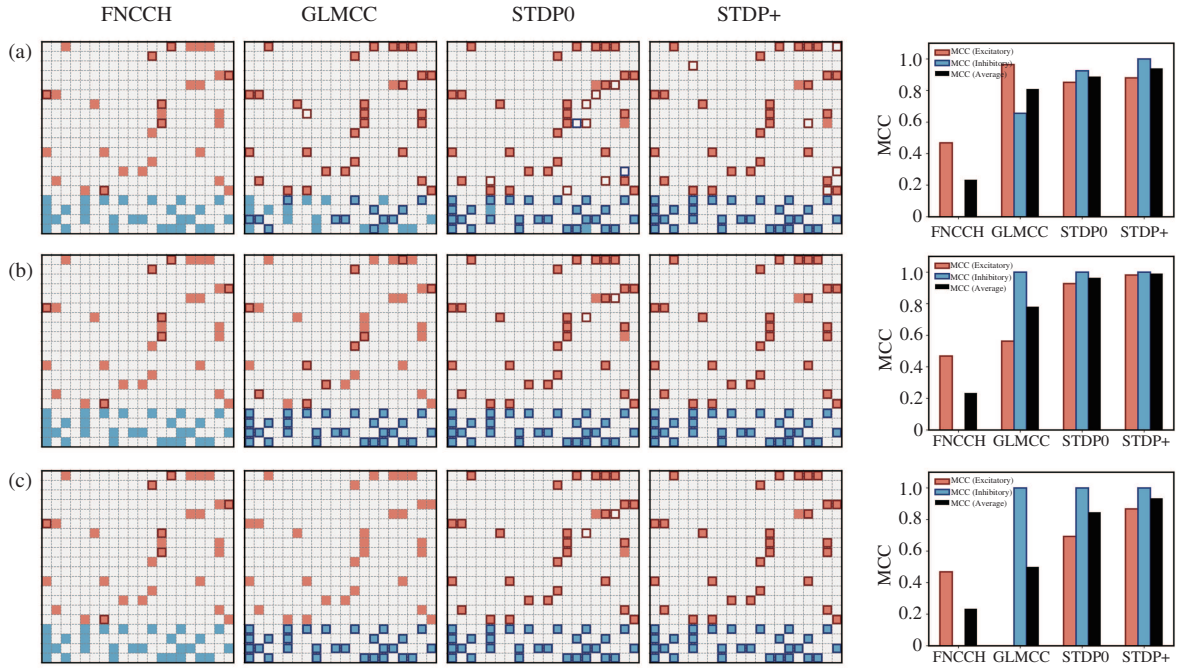


Figure 3 (Color online) Effect of transmission delay mismatch. (a) Connectivity matrices and inference accuracy in terms of MCC with the underestimated value of transmission delay, 2 ms. (b) Connectivity matrices and inference accuracy in terms of MCC with the correct value of transmission delay, 3 ms. (c) Connectivity matrices and inference accuracy in terms of MCC with the overestimated value of transmission delay, 4 ms.

For a fair comparison with the statistics-based inference methods, the neural spike data in [13] are used to test and evaluate STDP-based inference methods' performance. The network consists of 800 excitatory neurons and 200 inhibitory neurons. The excitatory neurons are connected to 12.5% of other neurons with log-normal distributed synaptic weights. The inhibitory neurons are connected to 25% of other neurons with normal distributed synaptic weights. The details of the analog-weighted neural network with HH neurons can be found in [13]. Figures 4(a) and (b) show the estimated connectivity matrices and the inference accuracy in MCC terms, respectively. The STDP+ method and GLMCC can infer most excitatory and inhibitory connections with relatively strong synaptic weights. The STDP0 method, however, estimates every connection to be inhibitory, which means it fails to distinguish the inhibitory connections from others. In contrast to the small performance gap between the STDP0 and STDP+ methods in the ternary-weighted neural network with LIF neurons, the STDP+ method shows much higher inference accuracy than the STDP0. This behavior can be attributed to a larger variation of the analog-weighted neural network's firing rate, 2.21 ± 1.03 Hz, compared to the ternary-weighted neural network, 4.62 ± 0.28 Hz. Without compensating for the different firing rates of neurons in the network, the final conductance obtained from STDP0 is primarily affected by the number of conductance updates, which is in turn determined by the post-synaptic neuron's firing rate, rather than the strength of excitatory or inhibitory connections. This effect is more severe when the iSTDP rule is applied to the memristor array since iSTDP with only depression updates cannot produce balanced conductance updates as eSTDP which offers both potentiation and depression updates.

Figure 4(c) shows the averaged MCCs for different inference methods with respect to the simulation time length. The STDP+ and the GLMCC clearly outperform other methods in the analog weight network case. While the GLMCC is specialized in estimating the analog synaptic weights, the STDP+ predicts the probability of connection from the device conductance updated by the STDP learning rule to produce an estimated binary connectivity matrix with a low computational cost. Since the excitatory synaptic weights follow the log-normal distribution, the large amounts of excitatory connections with weak synaptic strength in fact have minimal effects on the neurons' activation compared to the small number of strong excitatory connections. Thus, it is important for the inference methods to correctly infer the strong excitatory connections, not just producing an acceptable average MCC value for all connections. Figure 4(d) shows the MCC for excitatory connections with different minimum threshold values used to classify the connections. Excitatory connections weaker than the minimum threshold value

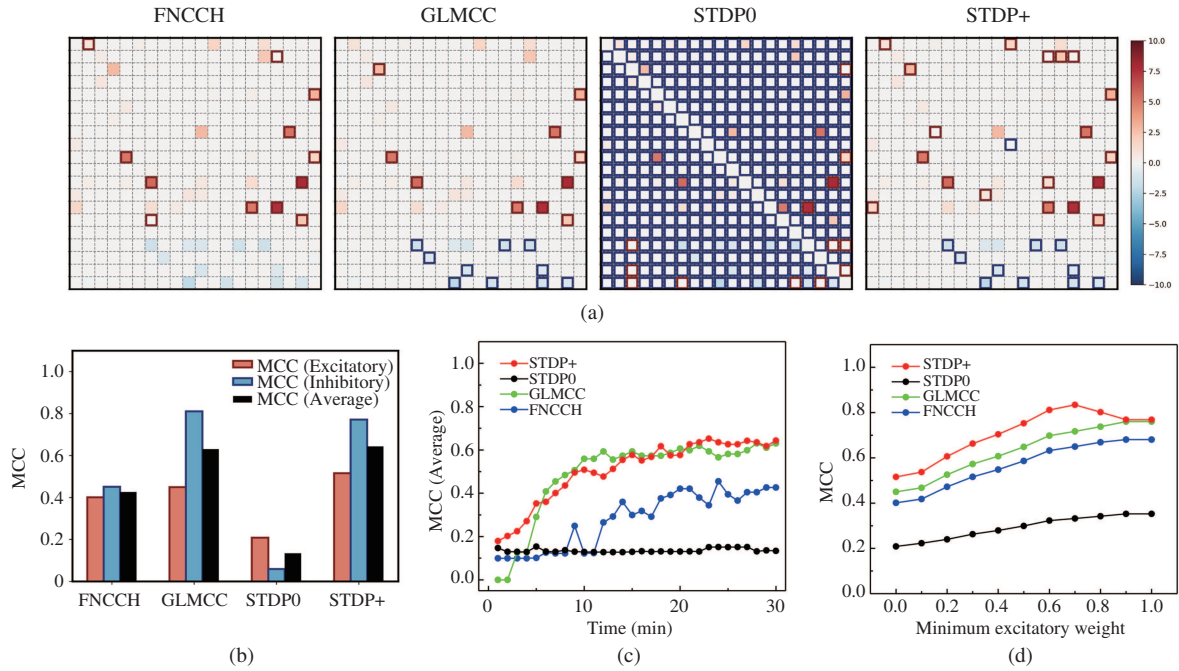


Figure 4 (Color online) Analog-weighted neural network with HH neurons. (a) Connectivity matrices with the ground truth (pixel) and the inferred connections (excitatory: red square, inhibitory: blue square). (b) Inference accuracy in terms of MCC. Averaged MCC is a mean of MCC for excitatory and MCC for inhibitory. (c) Averaged MCCs with respect to the simulation time length. (d) MCC for excitatory with respect to the different minimum threshold values for excitatory weights.

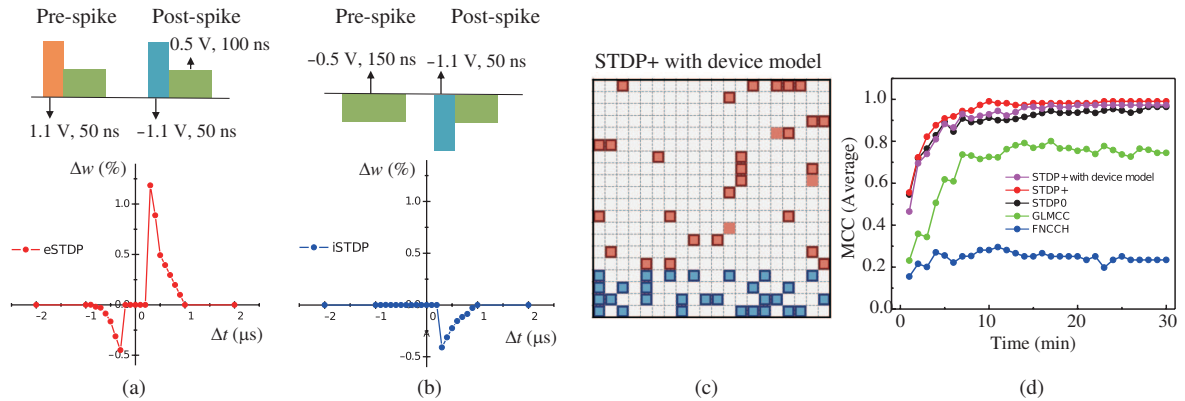


Figure 5 (Color online) Second-order memristor array for connectivity inference. (a) Voltage pulse configuration for eSTDP and eSTDP obtained from the circuit simulation. (b) Voltage pulse configuration for iSTDP and iSTDP obtained from the circuit simulation. (c) Connectivity matrix with the ground truth (pixel) and the inferred connections of STDP-based inference method with device model (excitatory: red, inhibitory: blue). (d) Averaged MCCs with respect to the simulation time length.

are ignored when the true positive cases for excitatory connections are calculated. By focusing on the inference of only strong excitatory connections, the performances of all methods are improved, and the STDP+ method outperforms all other methods highlighting the capability of this approach to pick up causality among the recorded signals. The improvement of inference accuracy for inhibitory connection is not significant since it follows a normal distribution which is not as long-tailed as the log-normal distribution.

The second-order memristor model [14–16] with coupled differential equations can comprehensively explain the switching mechanism of memristor devices and accurately predict the memristor’s dynamic behavior. By utilizing the temporal dynamics of the 2nd-state variable, i.e., the internal device temperature, the STDP behavior can be reproduced without any overlapped voltage pulse. Thus, the STDP-based inference methods can be natively implemented in an array composed of 2nd-order memristors. Figures 5(a) and (b) show the voltage pulse configuration for eSTDP and iSTDP, and the simulated eSTDP and iSTDP learning rules using the physical device model, where the pre-spike and post-spike

are applied to the top electrode and the bottom electrode of the memristor, respectively.

In eSTDP, when the post-spike comes after the pre-spike, the memristor conductance is potentiated as the total pulse sequence, including the positive heat pulse of the pre-spike followed by the positive programming voltage of the post-spike at the elevated temperature, induces enhanced SET programming. In iSTDP, to produce only depression update, the pre-spike consists of only the heat pulse, which induces enhanced RESET programming when the negative programming pulse of post-spike arrives after the pre-spike. Since the memristor's internal dynamics occur at a much faster time scales, a few μs ., the time scale of neural spike trains can be converted to the time scale of the memristor device by reducing the scale by a factor of 10000. Figures 5(c) and (d) show the ternary-weighted neural network's connectivity matrix inferred by 2nd-order memristor device array when using the physical device model, and the averaged MCCs with respect to the simulation time length. Although the STDP learning curves obtained from the circuit simulation using the device model are not exactly the same as the ideal STDP learning curves shown in Figure 1(d), comparable inference accuracy results can still be obtained. To allow the memristor network to directly process the neural spikes, the characteristic time of the memristor's internal dynamics needs to be slowed down to $\sim\text{ms}$ from $\sim\mu\text{s}$. This can possibly be achieved through device structure optimizations to control the internal temperature dynamics by managing the heat dissipation. For example, by inserting a heat insulating layer or a heat reservoir to prevent fast heat dissipation, or changing the switching layer or the base layer's material to tailor the specific heat or thermal conductivity. Memristor devices based on the migration of other ionic species will also be considered, as recent developments on perovskite halide-based memristors [25] have shown short-time dynamics on the order of a few tens of ms time scale, which is comparable with that of the biological neurons.

4 Conclusion

In this paper, the neural connectivity patterns, including the type and the direction of the synaptic connections, are inferred by STDP-based methods. For ternary-weighted neural networks with LIF neurons, the STDP-based inference methods not only show better accuracy but also strong tolerance to fluctuations in transmission delays when compared with statistics-based methods. When the synaptic weights are analog, such as log-normal or normal distributed, the proposed STDP-based inference methods have comparable accuracy to the statistics-based methods at a reduced computational cost. Since the STDP rules can be natively implemented in second-order memristors, the proposed approach can potentially be implemented cheaply using arrays of second-order memristors with minimal pre- and postprocessing.

The variation-tolerance and simplified computation can be attributed to the online and local learning property of the STDP rule. Rather than estimating the causality in the global profile of the cross-correlogram, the STDP-based inference methods update the possibility of connections based on the time sequence of the local spike pairs. When natively implemented in a second-order memristor, the computational cost/time can be further reduced compared with software-based STDP implementations. To experimentally implement the STDP-based methods in the second-order memristor array, the discrepancy between the ideal device model and the experimental results, as well as nonideal effects such as device-to-device variations need to be comprehensively analyzed. Successful implementations of the STDP algorithm on neural connectivity inference may encourage further theoretical studies on the use of local learning rules such as STDP in other tasks, and stimulate the development of new applications based on bio-inspired features.

Acknowledgements This work was supported in part by National Science Foundation through Award (Grant No. 1915550). The authors would like to thank Dr. S. H. Lee and Dr. M. Zidan for stimulating discussions.

References

- Insel T R, Landis S C, Collins F S. The NIH brain initiative. *Science*, 2013, 340: 687–688
- Amunts K, Ebell C, Muller J, et al. The human brain project: creating a European research infrastructure to decode the human brain. *Neuron*, 2016, 92: 574–581
- Okano H, Sasaki E, Yamamori T, et al. Brain/MINDS: a Japanese national brain project for marmoset neuroscience. *Neuron*, 2016, 92: 582–590
- Brown E N, Kass R E, Mitra P P. Multiple neural spike train data analysis: state-of-the-art and future challenges. *Nat Neurosci*, 2004, 7: 456–461
- Pillow J W, Shlens J, Paninski L, et al. Spatio-temporal correlations and visual signaling in a complete neuronal population. *Nature*, 2008, 454: 995–999
- de Abril I M, Yoshimoto J, Doya K. Connectivity inference from neural recording data: challenges, mathematical bases and research directions. *Neural Netw*, 2018, 102: 120–137

- 7 Garofalo M, Nieuw T, Massobrio P, et al. Evaluation of the performance of information theory-based methods and cross-correlation to estimate the functional connectivity in cortical networks. *PLoS ONE*, 2009, 4: 6482
- 8 Salinas E, Sejnowski T J. Correlated neuronal activity and the flow of neural information. *Nat Rev Neurosci*, 2001, 2: 539–550
- 9 Kraskov A, Stögbauer H, Grassberger P. Estimating mutual information. *Phys Rev E*, 2004, 69: 066138
- 10 Schreiber T. Measuring information transfer. *Phys Rev Lett*, 2000, 85: 461–464
- 11 Ito S, Hansen M E, Heiland R, et al. Extending transfer entropy improves identification of effective connectivity in a spiking cortical network model. *PLoS ONE*, 2011, 6: 27431
- 12 Pastore V P, Massobrio P, Godjoski A, et al. Identification of excitatory-inhibitory links and network topology in large-scale neuronal assemblies from multi-electrode recordings. *PLoS Comput Biol*, 2018, 14: 1006381
- 13 Kobayashi R, Kurita S, Kurth A, et al. Reconstructing neuronal circuitry from parallel spike trains. *Nat Commun*, 2019, 10: 1–13
- 14 Kim S, Choi S H, Lu W. Comprehensive physical model of dynamic resistive switching in an oxide memristor. *ACS Nano*, 2014, 8: 2369–2376
- 15 Kim S, Du C, Sheridan P, et al. Experimental demonstration of a second-order memristor and its ability to biorealistically implement synaptic plasticity. *Nano Lett*, 2015, 15: 2203–2211
- 16 Lee S H, Moon J, Jeong Y J, et al. Quantitative, Dynamic TaO_x memristor/resistive random access memory model. *ACS Appl Electron Mater*, 2020, 2: 701–709
- 17 Bi G Q, Poo M M. Synaptic modifications in cultured hippocampal neurons: dependence on spike timing, synaptic strength, and postsynaptic cell type. *J Neurosci*, 1998, 18: 10464–10472
- 18 Caporale N, Dan Y. Spike timing-dependent plasticity: a Hebbian learning rule. *Annu Rev Neurosci*, 2008, 31: 25–46
- 19 Diehl P U, Cook M. Unsupervised learning of digit recognition using spike-timing-dependent plasticity. *Front Comput Neurosc*, 2015, 9: 99
- 20 Kheradpisheh S R, Ganjtabesh M, Thorpe S J, et al. STDP-based spiking deep convolutional neural networks for object recognition. *Neural Netw*, 2018, 99: 56–67
- 21 Gewaltig M O, Diesmann M. NEST (neural simulation tool). *Scholarpedia*, 2007, 2: 1430
- 22 Song S, Sjöström P J, Reigl M, et al. Highly nonrandom features of synaptic connectivity in local cortical circuits. *PLoS Biol*, 2005, 3: 68
- 23 Hoffmann J H O, Meyer H S, Schmitt A C, et al. Synaptic conductance estimates of the connection between local inhibitor interneurons and pyramidal neurons in layer 2/3 of a cortical column. *Cereb Cortex*, 2015, 25: 4415–4429
- 24 Matthews B W. Comparison of the predicted and observed secondary structure of T4 phage lysozyme. *Biochim Biophys Acta (BBA) Protein Structure*, 1975, 405: 442–451
- 25 Zhu X, Wang Q, Lu W D. Memristor networks for real-time neural activity analysis. *Nat Commun*, 2020, 11: 2439